Long-QT syndrome-related sodium channel mutations probed by the dynamic action potential clamp technique

Géza Berecki[1,2], Jan G. Zegers[2], Zahurul A. Bhuiyan[3], Arie O. Verkerk[1,2], Ronald Wilders[2] and Antoni C. G. van Ginneken[1,2]

[1]*Experimental and Molecular Cardiology Group and the Departments of* [2]*Physiology and* [3]*Clinical Genetics, Academic Medical Center, University of Amsterdam, the Netherlands*

Long-QT3 syndrome (LQT3) is linked to cardiac sodium channel gene (*SCN5A*) mutations. In this study, we used the 'dynamic action potential clamp' (dAPC) technique to effectively replace the native sodium current (I_{Na}) of the Priebe–Beuckelmann human ventricular cell model with wild-type (WT) or mutant I_{Na} generated in a human embryonic kidney (HEK)-293 cell that is voltage clamped by the free-running action potential of the ventricular cell. We recorded I_{Na} from HEK cells expressing either WT or LQT3-associated Y1795C or A1330P *SCN5A* at 35°C, and let this current generate and shape the action potential (AP) of subepicardial, mid-myocardial and subendocardial model cells. The HEK cell's endogenous background current was completely removed by a real-time digital subtraction procedure. With WT I_{Na}, AP duration (APD) was longer than with the original Priebe–Beuckelmann model I_{Na}, due to a late I_{Na} component of ∼30 pA that could not be revealed with conventional voltage-clamp protocols. With mutant I_{Na}, this late component was larger (∼100 pA), producing a marked increase in APD (∼70–80 ms at 1 Hz for the subepicardial model cell). The late I_{Na} magnitude showed reverse frequency dependence, resulting in a significantly steeper APD–frequency relation in the mutant case. AP prolongation was more pronounced for the mid-myocardial cell type, resulting in increased APD dispersion for each of the mutants. For both mutants, a 2 s pause following rapid (2 Hz) pacing resulted in distorted AP morphology and beat-to-beat fluctuations of I_{Na}. Our dAPC data directly demonstrate the arrhythmogenic nature of LQT3-associated *SCN5A* mutations.

(Received 12 August 2005; accepted after revision 27 October 2005; first published online 27 October 2005)
Corresponding author G. Berecki: Department of Experimental Cardiology, Academic Medical Center, University of Amsterdam, Room M01-217, Meibergdreef 9, 1105 AZ Amsterdam, PO Box 22700, 1100 DE Amsterdam, The Netherlands. Email: g.berecki@amc.uva.nl

The human cardiac Na^+ channel (hH1), encoded by the *SCN5A* gene, is primarily responsible for the initiation and propagation of cardiac action potentials (APs). Mutations in *SCN5A* have long been known to cause a variety of cardiac rhythm disorders, including type 3 of the congenital long-QT (LQT3) syndrome (Jiang *et al.* 1994; Wang *et al.* 1995). It is accepted that the LQT3 arises from a delayed repolarization of the ventricular myocytes, due to a shift in the delicate balance between inward and outward currents during the plateau of the AP (Bennett *et al.* 1995), leading to an increased propensity for ventricular tachyarrhythmias and sudden arrhythmic death (Moss *et al.* 1995); for instance, an increase of Na^+ influx during depolarized membrane potentials is proposed to impair membrane repolarization, and thus render APs more prolonged.

At present, most effort has been devoted to documenting the effects of identified mutations on amplitudes and kinetics of various sodium currents (I_{Na}) upon heterologous expression, and the consequences of channelopathies for cardiac function are inferred by extrapolation (Wehrens *et al.* 2002). Advanced computer models of the ventricular AP can link a genetic defect to its cellular phenotype in a cardiac arrhythmia (Clancy & Rudy, 1999). However, since voltage-gated cardiac Na^+ channels ($Na_V1.5$) are often studied under conditions that severely affect gating (e.g. room temperature), the mathematical description of channel kinetics can be difficult when mutations have subtle effects on I_{Na}. Furthermore, the time-course of I_{Na} during square voltage-clamp steps is different from what is recorded during an AP. This is explained by the fact that $Na_V1.5$ channels not only open and inactivate rapidly during depolarization, but also reopen during the plateau and repolarization phases, carrying 'persistent' or 'late' inward current (late I_{Na}). Late I_{Na} has been demonstrated in

 DOI: 10.1113/jphysiol.2005.096578

cardiac ventricular specimens of various mammalian species including humans (Maltsev *et al.* 1998), and its role has been documented in the generation of normal as well altered AP durations. Recent studies strongly suggest that complex features of SCN5A channel kinetics can best be studied during physiological voltage waveforms (Clancy *et al.* 2003; Magyar *et al.* 2004).

With the dynamic action potential clamp (dAPC) technique (Berecki *et al.* 2005), the contribution of wild-type (WT) and mutated channels to the AP morphology can be determined without making assumptions regarding kinetic properties of the channels. With the dAPC approach, the original I_{Na} of a ventricular cell can effectively be replaced by I_{Na} recorded from a transfected human embryonic kidney (HEK)-293 cell that is voltage clamped by the free-running AP of the ventricular cell. To this end, I_{Na} of the Priebe–Beuckelmann (PB) human ventricular cell model (Priebe & Beuckelmann, 1998) is replaced with HEK cell I_{Na} applied to the ventricular cell model as an external current input. When WT HEK cell I_{Na} is added to the net membrane current of this ventricular cell, the resulting AP should be considered as 'normal', whereas a mutant HEK cell I_{Na} should cause distortion of the AP.

We hypothesize that rapid and refined interpretation of the altered SCN5A channel function and changed AP morphology is possible with an experimental setting in which mutant channels are allowed to follow a 'natural' time-course of membrane potential (V_m) change, while they are simultaneously allowed to contribute current to the AP as they would have when incorporated into a real ventricular cell. In this study, we assess the functional implications of Y1795C and A1330P missense mutations, associated with 'classic' LQT3 gain-of-function phenotypes caused by distinct molecular mechanisms: the Y1795C mutation (substitution of a tyrosine by a cysteine) leads to dysfunction by slowing the onset of inactivation and causing channel bursting that significantly increases late I_{Na} at depolarized membrane potentials (Rivolta *et al.* 2001; Clancy *et al.* 2002), while the A1330P mutation (substitution of an alanine to proline) results in a positive shift in the voltage dependence of inactivation, a slowing of the time-course of inactivation, and a faster recovery from inactivation rather than a late I_{Na} (Wedekind *et al.* 2001). These changes in kinetics are thought to severely disrupt cellular repolarization and lead to AP prolongation. Computer simulations (Clancy *et al.* 2002) based on the 'dynamic Luo-Rudy' (LRd) model of a ventricular cell suggest that the *Y1795C* mutation, if expressed homozygously, increases APD by 10–25 ms (at 2 and 1 Hz, respectively).

We took advantage of the dAPC approach to directly establish effects of various clinically relevant stimulation frequencies, as well the consequence of a pause, on AP morphology and on the time-course and magnitude of late I_{Na} during the plateau and repolarizing phases of the AP.

Methods

Plasmid construction

Site-directed (tyrosine to cysteine) mutagenesis was performed on the *SCN5A* α-subunit cDNA cloned into pSP64T. The Y1795C cDNA was then subcloned using the *Hind*III–*Xba*I sites of the expression vector pCGI for bicistronic expression of the channel protein and GFP reporter in HEK cells. The *A1330P* cDNA was prepared as previously described (Wedekind *et al.* 2001). To express WT or mutant hH1, HEK cells were transiently cotransfected with 1 μg of Na^+ channel α-subunit cDNA and 1 μg hβ_1-subunit cDNA using lipofectamine (Gibco BRL, Life Technologies, Scotland) and cultured at 37°C.

Electrophysiology

HEK cells were superfused with a solution containing (mM): NaCl 140, CsCl 10, $CaCl_2$ 2, $MgCl_2$ 1, glucose 5, sucrose 10, Hepes 10 (pH 7.4 with NaOH). Patch pipettes (1–1.2 MΩ tip resistance) were filled with a solution containing (mM): CsCl 10, CsF 110, NaF 10, EGTA 11, $CaCl_2$ 1, $MgCl_2$ 1, Na_2ATP 2, Hepes 10 (pH 7.3 with CsOH). The pH of solutions was corrected for temperature; potentials were corrected for liquid junction potential; and osmolarity was measured with a semimicro osmometer (Knauer, Berlin). Membrane currents were recorded with an Axopatch 200B amplifier (Axon Instruments, Inc., Union City, CA, USA) in the whole-cell configuration of the patch-clamp technique, at 35 ± 0.5°C. Series resistance (R_s) values, typically of 2–2.5 MΩ, were 90–95% compensated. To minimize possible voltage errors, small HEK cells of 8–12 pF cell capacitance ($C_m = 10.4 \pm 0.04$, $n = 33$), expressing peak I_{Na} amplitudes < 10 nA were selected (Nagatomo *et al.* 1998). With the given R_s and C_m values, the true membrane potential could be established within about 25 μs after the start of the step command without overshoot or ringing (Sigworth, 1983), fast enough to voltage clamp rapid ionic currents. The estimated residual (uncompensated) R_s of < 200 kΩ could theoretically cause a < 2 mV voltage error in the membrane potential relative to the command potential in the presence of 10 nA amplitude I_{Na}. Currents and potentials were low-pass filtered (cut-off frequency 5 or 10 kHz) and digitized at 20 kHz. Voltage control, data acquisition and analysis were accomplished using custom software. In the experiments using TTX, I_{Na} was determined as the current blocked by 50 μM TTX (Alomone Laboratories, Israel). Only those data were analysed in which no shift in holding current at −90 mV was observed during TTX superfusion. To quantify late

I_{Na}, the largest inward current amplitude was measured during a sustained step depolarization or during phase 2 (plateau) or 3 (rapid repolarization) of the AP.

Dynamic action potential clamp

The overall design of the dAPC technique is represented in Fig. 1*A*. A single cardiac ventricular cell and a transfected HEK cell can be electrically coupled by means of an electrical circuit. The ventricular cell is in current clamp mode on one patch-clamp setup, whereas the HEK cell is in voltage-clamp mode on another setup. The command potential for the HEK cell is the free-running V_m of the ventricular cell ('action potential clamp'), and the input I_{Na} applied to the ventricular cell is the I_{Na} recorded from the transfected HEK cell, a connection resulting in the dAPC condition (Berecki *et al.* 2005). We used the model cell variant of the dAPC technique (Fig. 1*B*) to (partly) replace the I_{Na} of the human ventricular PB cell model with transiently expressed SCN5A I_{Na} (see below). DynaClamp, the user program for dAPC, allows a guaranteed-timing real-time process (i.e. 40 μs periodic time steps with the PB cell model), and allows scaling of the model cell currents and that of input I_{Na} to any desired magnitude. In the original PB cell model, peak amplitude of the native I_{Na} during the AP upstroke is ~58.3 nA (380 A F^{-1}, at 1 Hz) and the late I_{Na} component is not implemented. Reducing the ventricular

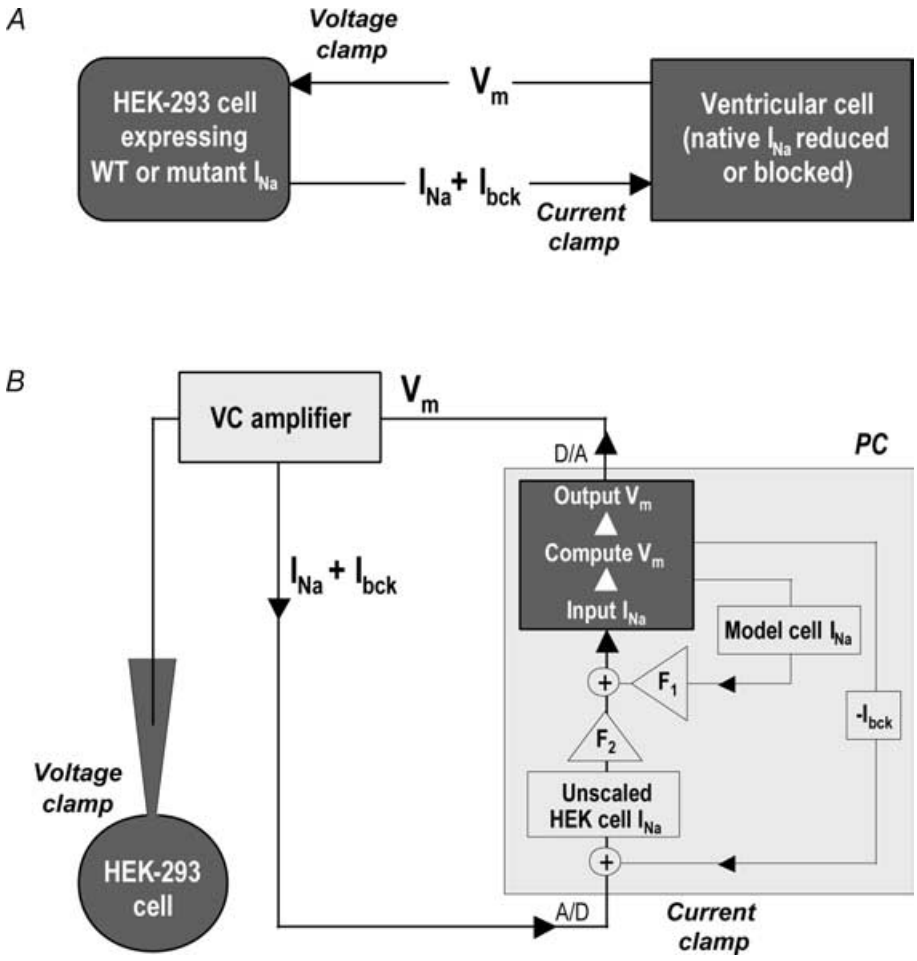

Figure 1. Dynamic action potential clamp (dAPC) technique
A, general experimental design. The cardiac ventricular cell is in current clamp. The *SCN5A* cDNA-transfected HEK cell is voltage clamped with V_m of the ventricular cell. I_{Na} from the HEK cell is continuously applied to the ventricular cell as an external current input, partly or entirely replacing I_{Na} in the myocyte. *B*, model cell mode of dAPC technique: after real-time digital subtraction of HEK cell I_{bck}, I_{Na} from the HEK cell is scaled by factor F_2; model cell I_{Na} density is reduced to 40% of the original value (scaling factor F_1). The I_{Na} of the PB model cell incorporates a 'heterozygous' I_{Na} composed of reduced model cell I_{Na} and scaled HEK cell (input) I_{Na}(+). The V_m of the human ventricular cell model is computed in real time using the thus-obtained I_{Na} and applied as voltage-clamp command potential to the HEK cell, thus establishing dAPC.

Table 1. Action potential parameters of the human ventricular 'subepicardial' model cell with WT, Y1795C, and A1330P I_{Na}

	1 Hz			2 Hz		
	WT ($n = 11$)	Y1795C ($n = 8$)	A1330P ($n = 6$)	WT ($n = 8$)	Y1795C ($n = 7$)	A1330P ($n = 6$)
Overshoot (mV)	34.3 ± 0.7	33.8 ± 1.8	32.8 ± 0.8	33.2 ± 1.2	32.3 ± 1.4	30.8 ± 0.4
MDP (mV)	−91.2 ± 0.1	−91.8 ± 0.3	−91.5 ± 0.3	−90.2 ± 0.2	−89.4 ± 0.4	−90.5 ± 0.4
APA (mV)	125.5 ± 0.7	125.6 ± 2.0	124.3 ± 0.8	123.4 ± 1.1	121.7 ± 1.6	121.3 ± 0.7
V_{max} (V s^{-1})	263.5 ± 7.7	262.5 ± 15.3	259.2 ± 8.5	251.3 ± 5.9	251.0 ± 9.9	248.0 ± 5.2
APD_{20} (ms)	6.4 ± 0.3	7.0 ± 0.8	7.3 ± 0.8	6.0 ± 0.3	7.3 ± 1.1	7.4 ± 0.9
APD_{50} (ms)	312.3 ± 3.2	389.9 ± 13.8*	409.3 ± 19.7*	281.5 ± 2.3	306.1 ± 7.3*	301.1 ± 12.1
APD_{90} (ms)	404.7 ± 3.7	475.6 ± 16.1*	486.0 ± 17.0*	366.5 ± 1.8	401.2 ± 8.9*	379.7 ± 9.8
PA_{20} (mV)	10.2 ± 0.1	11.6 ± 0.2*	16.1 ± 0.9*	10.4 ± 0.1	10.5 ± 0.2	14.8 ± 1.0*
PA_{60} (mV)	18.0 ± 0.1	20.3 ± 0.6	25.6 ± 1.8*	17.8 ± 0.2	17.3 ± 0.4	22.3 ± 1.5*

MDP, maximum diastolic potential; APA, action potential amplitude; V_{max}, maximum upstroke velocity; APD_{20}, APD_{50}, and APD_{90}, AP duration at 20, 50, and 90% repolarization, respectively; PA_{20} and PA_{60}, plateau amplitude at 20 and 60 ms repolarization, respectively. Values are mean ± S.E.M. *Significant difference *versus* control ($P < 0.05$ for mutant *versus* WT).

cell's original (peak) I_{Na} density by 34% or 60% results in proportionate model cell AP upstroke velocity decreases. At the same time, these gradual I_{Na}-density reductions do not have APD-shortening effects at physiologically relevant stimulation rates (see Supplemental Fig. S1). In all dAPC experiments, we used 40% of model cell I_{Na} density (152 A F^{-1}, at 1 Hz), combined with the implemented HEK cell (input) I_{Na}, the peak amplitude of which was up scaled to ∼20 nA (∼130 A F^{-1}). The resulting (combined) I_{Na}s provided realistic rates of membrane depolarizations (Table 1) and approach the heterozygous I_{Na} expression in carriers of LQT3 mutations. When scaling input I_{Na}, we first determined the maximal I_{Na} amplitude in voltage-clamped HEK cells during 30 ms depolarizing voltage steps to voltages ranging from −60 to +10 mV (from a holding potential, $V_{hold} = -90$ mV, in 10 mV steps). Here, graded activation of the I_{Na} during voltage steps also served as an index for reliable voltage control (Nagatomo *et al.* 1998). We then used the largest I_{Na} amplitude value to estimate the scaling factor (F_2) for current input to the PB model cell (Fig. 1*B*). In order to minimize the endogenous HEK cell 'background' currents (I_{bck}), as well as noise from several sources including the operational amplifier and associated circuitry, F_2 values were kept below 3. Experiments requiring $F_2 > 3$ were rejected. To further improve recording conditions, it proved necessary to develop a procedure to compute and real-time subtract I_{bck} (see Results). Having completed the described preparative steps, the program could establish dAPC configuration between the ventricular cell and the HEK cell. For this, a series of 2 ms, 4 nA, suprathreshold stimuli were applied to the ventricular cell model at a fixed rate, for 10 s. At each stimulus, the V_m of the HEK cell followed that of the model cell. Suprathreshold stimuli would thus generate I_{Na} in the HEK cell, which – along with 40% of original (cell model) I_{Na} – provided the inward current needed for the upstroke of the AP. Optionally, a 2 s pause was implemented during stimulation, starting at 5 s after onset of pacing. The combination of ionic currents of the model cell and WT I_{Na} of the HEK cell revealed APs, which could be considered as 'normal', representing healthy individuals. Using the same method for HEK cells containing mutant channels resulted in APs that were considered to be characteristic for cells from the ventricular tissue of a patient from which the mutant was derived.

Statistics

All values are represented as mean ± S.E.M. (n, number of cells). Two sets of data are considered significantly different if $P < 0.05$ in unpaired Student's t test or in one-way analysis of variance (ANOVA) followed by pair-wise comparison using the Holm–Sidak test.

Results

Real-time digital subtraction of HEK-293 cell background currents (I_{bck})

To adequately record and implement I_{Na} in dAPC experiments, I_{bck}-removal is essential. A large component of this current is carried through endogenous volume-regulated anion channels (Helix *et al.* 2003). A significant I_{bck}-reduction could first be obtained by adjusting the osmolarity of the extracellular solution with sucrose (to 310 mosmol l^{-1}, slightly hypertonic with respect to the 290 mosmol l^{-1} pipette solution) (not shown). We used square wave as well as various ramp and AP-shaped protocols to characterize the remaining I_{bck} in empty and transfected HEK cells (Fig. 2). At −90 mV, in most HEK cells I_{bck} amplitude was < 40 pA (32.4 ± 3.4 pA, $n = 11$) (Fig. 2*A*). AP-like

waveforms, consisting of a depolarizing step followed by a 0.43 V s^{-1} repolarizing ramp ('step-ramp'), were applied at 1 s inter-ramp intervals. The averaged I_{bck} traces during the ramp, plotted against V_m (Fig. 2*A*, right) resulted in I_{bck}–V relationships similar to that obtained with step protocols (Fig. 2*A*, left), and were not influenced by lengthening (to 2 s) or shortening (to 0.2 s) of the interramp intervals (not shown). The average current-voltage (I_{bck}–V) relationship shows that I_{bck} is slightly outwardly rectifying, reverses around 0 mV, and can be well-described with a third order polynomial equation:

$$I_{bck} = -0.38 + 0.52V_m + 3.69 \times 10^{-3}(V_m)^2 + 1.29 \times 10^{-5}(V_m)^3 \quad (1)$$

where I_{bck} is in picoamps, and V_m is in millivolts (Fig. 2*A*, left).

A step-ramp waveform, preceded by a 20 s voltage step to −50 or −60 mV, was implemented in dAPC experiments. The long depolarizing holding potential (V_{hold}) before the step-ramp served to inactivate I_{Na} (Fig. 2*B* and Supplemental Fig. S2), while the step-ramp allowed defining of I_{bck}–V relationships in (transfected) individual HEK cells. Figure 3 illustrates I_{bck} subtraction in a dAPC experiment. The ramp-evoked I_{bck}–V relationship is stored in a lookup table. Equation (1) is fitted to the data points between −120 and −70 mV, using a least squares fitting procedure and a scaling factor P as the only variable. Thus, the I_{bck} amplitude values for the whole voltage range are based on the scaled I_{bck}–V of non-transfected HEK cells (see Fig. 2*A*). This was done to avoid any possible interference of late I_{Na} for cases when I_{Na} inactivation during the 20 s V_{hold} of −60 or −50 mV was incomplete (see Supplemental Fig. S3). To assess the fit, offline results were generated in a separate file (Fig. 3*B*). In summary, when the program establishes dAPC condition, I_{bck} is characterized and then entirely subtracted from the input current, without affecting I_{Na}, including late components.

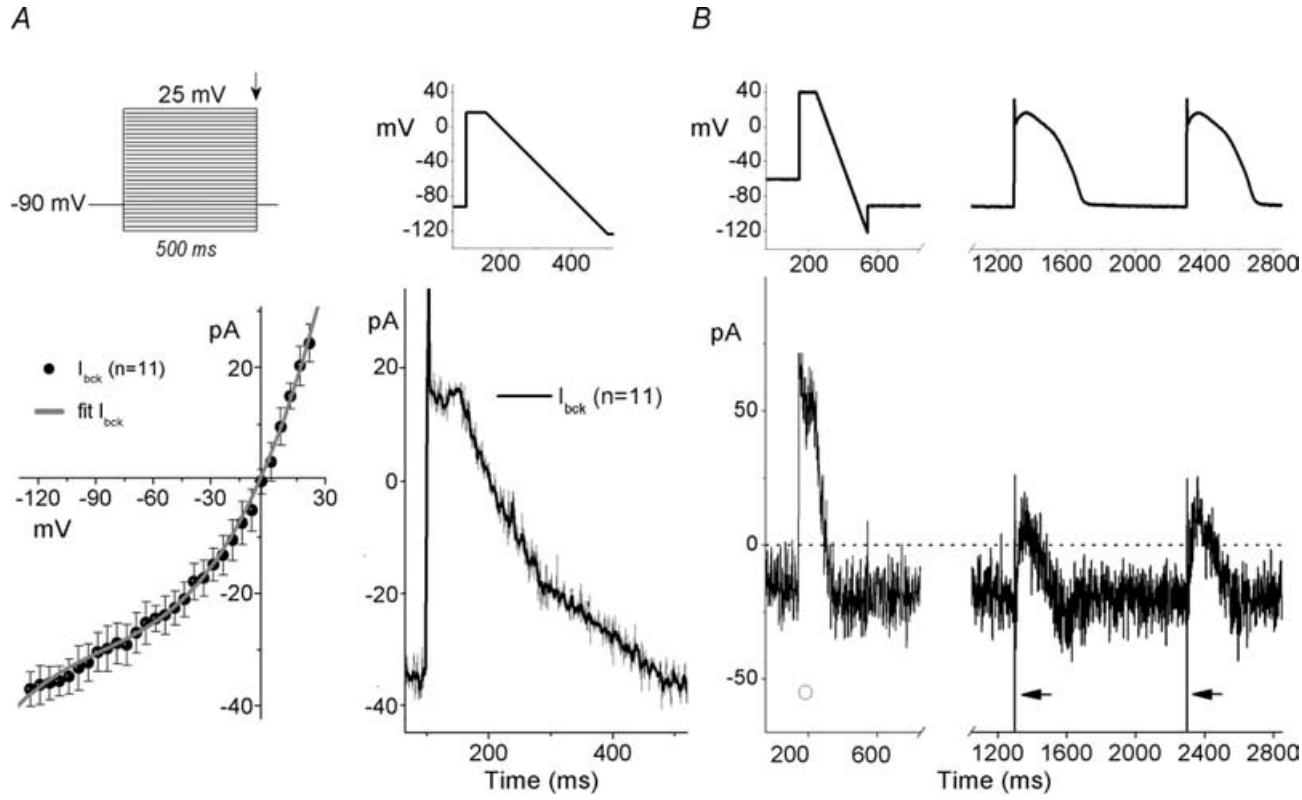

Figure 2. Square wave-, step-ramp-, and AP-elicited currents in HEK-293 cells
A, I_{bck} in non-transfected HEK cells. Upper left panel depicts the voltage-step protocol; lower left panel shows the corresponding I_{bck}–V, determined from amplitudes at the end of the 500-ms voltage steps (arrow). The fit (continuous line) is a third-order polynomial equation (see text for details). A step-ramp waveform (upper right panel) was used to determine time-course of averaged I_{bck} (lower right panel). *B*, step-ramp and 'subepicardial'-type AP-waveforms (top) to activate I_{bck} (bottom) in a WT *SCN5A* cDNA-transfected HEK cell (representative examples). Note the absence (○) and the presence (arrows) of fast I_{Na}, as a function of V_{hold} of −60 mV and −90 mV, respectively (see text for details). APs were generated using the PB model cell; broken line shows zero current level; peak I_{Na} is off scale.

Time-course of the WT and mutant Na^+ currents

Transient transfections of WT or mutant sodium channel subunits into HEK cells resulted in variable ion channel protein expression levels, with the highest I_{Na} amplitudes often exceeding 10 nA. We studied these currents in a series of conventional whole-cell voltage clamp experiments, at 35°C (Fig. 4). To demonstrate the effects of AP morphology on I_{Na}, we compared pairs of current traces evoked by a step depolarization, and subsequently by a PB model cell AP waveform (AP clamp). I_{Na}s were identified as TTX-sensitive current components obtained by digitally subtracting traces recorded before and after addition of 50 μM TTX. In these experiments, I_{bck} could also be identified as the TTX-resistant component. Within a cell, both depolarizing waveforms (step and AP) resulted in similar peak I_{Na} amplitudes (not shown). By using an AP waveform as voltage command, the TTX-sensitive late I_{Na} was detectable as an inward component during the plateau and repolarization phases in all tranfected cells. With a voltage step however, an inward late I_{Na} component could clearly be revealed only in cells transfected with the mutant channels.

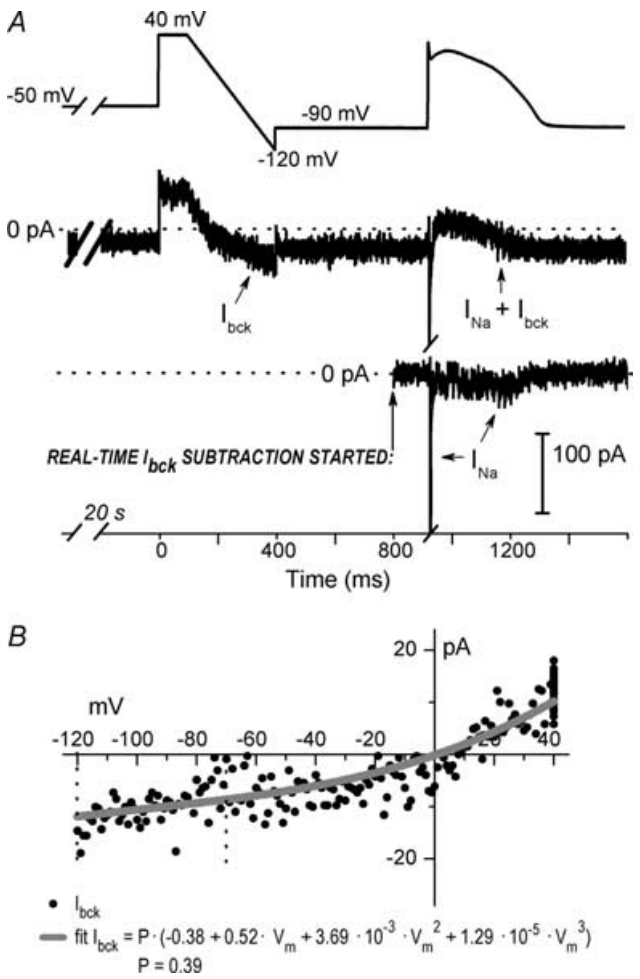

Figure 3. Real-time HEK-293 cell I_{bck} subtraction in a dAPC experiment, using a WT *SCN5A* cDNA-transfected HEK-293 cell
A, step-ramp voltage protocol and the first AP elicited in a subepicardial model cell. The maximum diastolic potential (MDP) during dAPC was −90 mV (top); Middle: I_{Na} in the presence of I_{bck} (arrows) and after I_{bck} removal (bottom). Note the transient WT late I_{Na} during AP repolarization. Broken line shows zero current level. *B*, *I–V* relationship of I_{bck} in the experiment shown in A, fit with the scaled polynomial equation ($P = 0.39$) (see text for details).

Replacing I_{Na} of the ventricular model cell with wild-type or mutant I_{Na}

To study the functional consequences of the *Y1795C* and *A1330P* mutations, we performed dAPC experiments by implementing WT or mutant I_{Na} in 'model cell mode' (Fig. 1*B*). With WT I_{Na}, APs were considered as 'normal', although they exhibited longer AP durations (APDs) than those of the original PB model (where, e.g. APD_{90} is ∼355 ms at 1 Hz) (Table 1). The inward current responsible for the additional prolongation originates from WT $Na_V1.5$ channel reopening that occurs under non-equilibrium conditions (Clancy *et al.* 2003); this mechanism is not implemented in the original PB model. To demonstrate that deleterious effects of LQT3 mutations preferentially occur at slow stimulation rates (Clancy *et al.* 2002; Nagatomo *et al.* 2002), and to investigate the effects of a pause on the APD and I_{Na}, we implemented a 2 s pause during pacing at various rates. The cellular repolarization–disruption effect of the *Y1795C* mutation is shown in Fig. 5. Time-course and amplitude of late I_{Na} show beat-to-beat fluctuations, probably due to the stochastic nature of $Na_V1.5$ channel openings (Zaniboni *et al.* 2000). Consistent with the complex gating mechanism of $Na_V1.5$ channels, both WT and mutant channels exhibit an inward late I_{Na} component during the AP plateau and repolarization phases. However, the Y1795C mutant clearly generates larger late I_{Na}s (∼80–120 pA) and longer APDs than the WT (∼25–30 pA) (Fig. 5, Table 1). When the AP prolongs, several current components of the model cell also undergo changes (Fig. 5*D*) that contribute to the shift in balance between inward (increased I_{Ca}) and outward (e.g. increased I_{Ks}) currents. The AP-prolonging effect of the A1330P mutation was evident only at slower pacing (Table 1). The effect of this mutation was moderate at 2 Hz, but also here, pause-dependent prolongation was clearly revealed (Fig. 6). Late I_{Na} became larger as the stimulation rate was slowed or after a pause, exaggerating the extent of AP prolongation. In traditional voltage-clamp experiments carried out at room temperature, several LQT3 mutants, including the Y1795C, display a progressive reduction of peak I_{Na} at fast stimulation rates (Rivolta *et al.* 2001). This was confirmed also by our dAPC data at physiological temperature,

which show that successive depolarizations within the pulse train result in a progressive decrease of the peak I_{Na} amplitudes to a (frequency-dependent) quasi steady-state value (Fig. 7). This decrease was more enhanced with mutant channels, suggesting a 'more absorbing' intermediate inactivation with both mutants. We analysed in detail AP characteristics of the epicardial model cell (Table 1), and plotted the frequency dependence of APD_{90} values generated with WT or mutant input I_{Na}s. (Fig. 8). For both WT and mutant I_{Na}s, APD_{90} values increased when pacing rate was reduced from 2 to 1 or 0.5 Hz as a result of adaptation (Franz *et al.* 1983). However, at 0.5 and 1 Hz, both mutations showed a more pronounced AP prolongation than WT, resulting in steeper APD–frequency relationships, demonstrating that deleterious effects preferentially occur at slow stimulation rates.

Action potential heterogeneity in the PB model cell with WT and mutant I_{Na}

The time-course of the late I_{Na} depends on the applied depolarizing voltage waveforms (Fig. 4). To investigate the effects of distinct AP morphologies on late I_{Na}, we generated mid-myocardial (M), and subendocardial cells by altering relative densities of selected membrane ionic currents in the 'subepicardial' PB model cell as described in our previous study (Berecki *et al.* 2005), and by implementing HEK cell I_{Na} to these cell models; the resulting APs were of different shape: AP heterogeneity (Supplemental Fig. S4*A*). Similar to results obtained with the subepicardial cell, the *Y1795C* and *A1330P* mutations caused AP prolongation also with 'subendocardial' and 'M' cells (Fig. 9). The mutation-induced APD-prolonging effects were most notable in M cells (Supplemental Fig. S4*B*

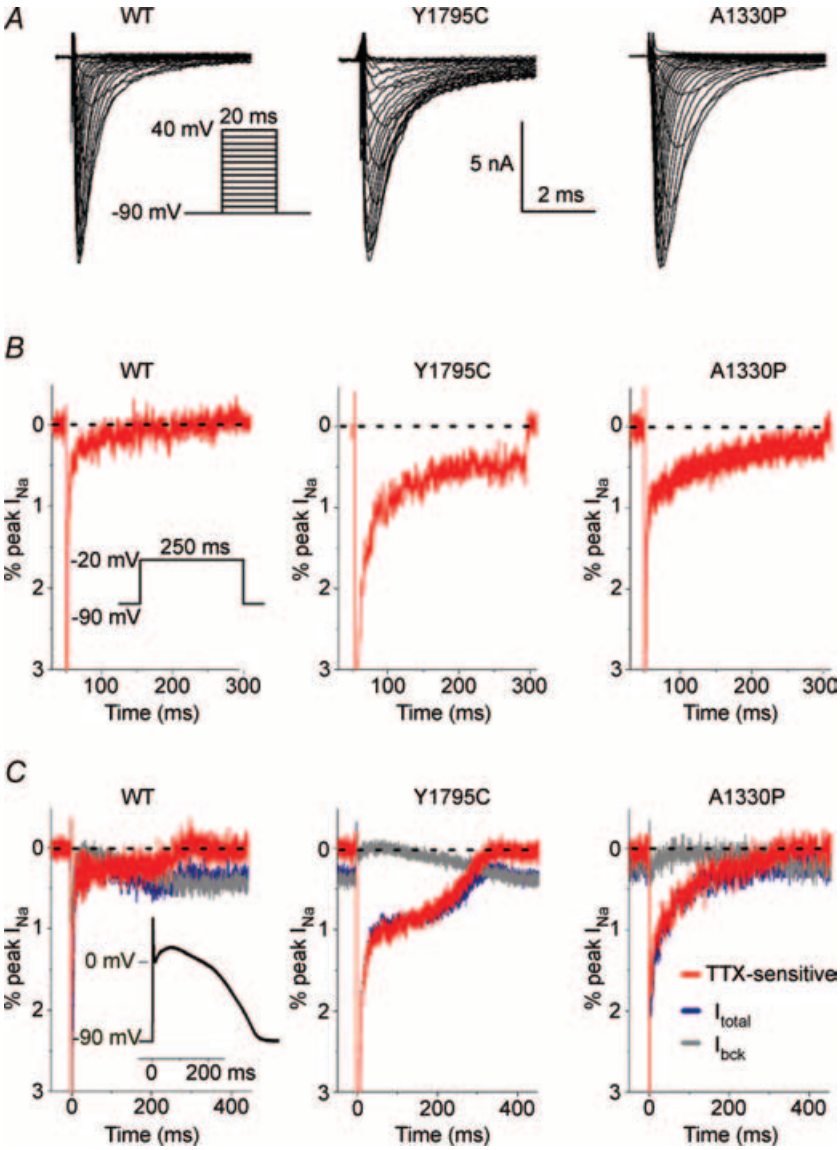

Figure 4. Whole-cell currents in HEK-293 cells transfected with WT, *Y1795C*, or *A1330P* cDNAs
A, representative I_{Na} traces. The voltage protocol is shown as an inset. Interpulse interval was 2 s. *B*, typical, 250 ms step depolarization-evoked TTX-sensitive whole-cell I_{Na} traces obtained by subtraction and plotted as percentage of peak I_{Na}; inset: protocol. Note that late I_{Na} is hardly detectable with WT SCN5A channels upon a step depolarization. Peak currents are off scale; broken lines indicate zero current level. *C*, superimposed tracing of AP clamp-evoked currents: control (I_{total}, blue), TTX-resistant (I_{bck}, grey), and difference (TTX-sensitive, red). Currents were plotted as percentage of peak I_{Na}; to record WT and mutant I_{Na} traces, the same cells were used as in *B*; in all cases I_{Na} was ~10 nA; peak currents are off scale; broken line shows zero current level. AP clamp waveform shown as inset.

and *C*), probably due to smaller repolarizing I_{Ks} densities in these cells. As a result, dispersion in AP duration was considerably larger for the mutants than for WT. At 1 Hz, the difference between longest (M cell) and shortest (epicardial cell) APD_{90} was ∼197 ms and ∼199 ms for the Y1795C and A1330P mutants, respectively, whereas it was ∼77 ms for WT (Supplemental Fig. S4*B*). When implementing mutant (Y1795C or A1330P) input I_{Na}, we were unable to perform dAPC experiments with the M cell at 2 Hz, since the evoked APs did not repolarize within 500 ms. Figure 9 further reveals a major difference with regard to the time-course of I_{Na} in the subendocardial and M cells, partly attributable to a change in driving force for Na^+ during the AP. With WT I_{Na} at 1 Hz, the plateau amplitude at 60 ms repolarization (PA_{60}) of the subendocardial cell is ∼28.1 mV, compared to that of ∼19.5 mV of the subepicardial and M cells (Supplemental Fig. S4*A*). The more depolarized plateau results in a decrease of the driving force for Na^+ (which in turn results in a smaller momentary late I_{Na}). This is easily traceable when comparing, e.g. time-courses of A1330P V_m and I_{Na} in the subendocardial and M cells (Fig. 9*A* and *B*). The arrows in Fig. 9 indicate the maximal PA and the corresponding late I_{Na} amplitudes in the subendocardial and M cells, respectively.

Discussion

The $Na_V1.5$ channel of the heart is a multisubunit protein complex composed of a single large α-subunit, SCN5A, along with one or more auxiliary β-subunits (Catterall,

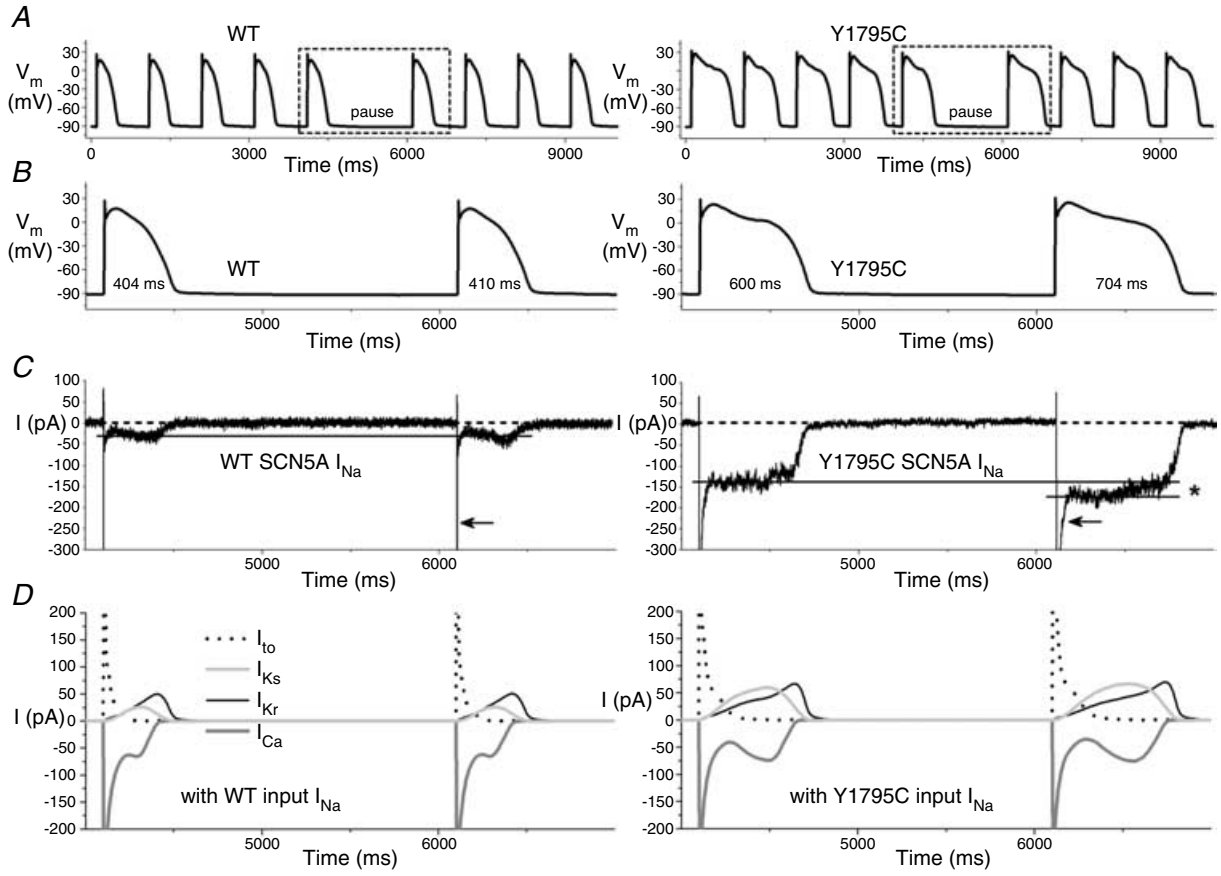

Figure 5. Dynamic action potential clamp with WT or Y1795C I_{Na}
A, subepicardial cell APs elicited at 1 Hz before and after a 2 s pause. APs with mutant I_{Na} are prolonged compared to WT (see Table 1). *B*, boxed APs from *A* and associated I_{Na} in *C*, on expanded time scale. HEK cell I_{Na}s were scaled to identical peak amplitudes (21 nA), and applied to the 'subepicardial' PB model cell as an external current input. Note that late I_{Na}-increase after the pause is more pronounced with the mutant (*). Broken line shows zero current level; peak I_{Na} is off scale; note the slower time-course of peak I_{Na}-inactivation of the mutant compared to the WT (arrows). *D*, relationship between the APs from *B* and selected membrane current components of the PB model cell, showing the changes in the time-course of transient outward K^+ current (I_{to}), slowly and rapidly activating components of the delayed rectifier K^+ current (I_{Ks} and I_{Kr}, respectively), and L-type Ca^{2+} current (I_{Ca}), along with changes in mutant I_{Na}.

2000), fine-tuned for the frequency and the waveform of APs (Ruff, 1998). The majority of LQT3-related mutations cause 'classic' gain-of-function due to a late inward I_{Na}, although in some LQT3-related *SCN5A* mutations this late I_{Na} seems to be absent (An *et al.* 1998; Wedekind *et al.* 2001; Rivolta *et al.* 2002; Smits *et al.* 2005), findings that suggest heterogeneity of mechanisms underlying the clinical phenotype of the syndrome.

In this study, we used dAPC technique to investigate the effects of LQT3-related sodium channelopathies in a cardiac (model) cell. This technique is an extension of the 'dynamic clamp' approach (Wilders, 2005), and has proven to be a powerful experimental tool allowing unique combinations of cardiac cells and an ion channel expression system (Berecki *et al.* 2005). The dAPC configuration generates a more physiological setting than the traditional methods of voltage clamp and AP clamp. During each cycle of a real-time feedback loop, membrane potential is calculated by solving ordinary differential equations and is in turn applied to the HEK-293 cell, altering the profile of the elicited I_{Na}. We scrutinized the time-course-, voltage- and frequency-dependence of transiently expressed WT and two mutant I_{Na}s, to directly establish the effects of two LQT3-related mutations on the ventricular (model) cell AP characteristics and on the time-course of the elicited I_{Na}. With this technique, kinetic features that remain unnoticed when standard voltage-clamp protocols are used become apparent. Our data directly support the idea that late I_{Na} importantly contributes to the AP plateau and plays a crucial role during AP repolarization, where non-equilibrium conditions enhance $Na_V1.5$ channel reopening.

Contrary to our previous dAPC study, where the implemented HERG current was downscaled making I_{bck} negligible (Berecki *et al.* 2005), in these experiments I_{Na} needed upscaling. This procedure would increase I_{bck} so that it would interfere with the late I_{Na} during the AP plateau. The very efficient I_{bck}-subtraction method introduced in this study made it possible to record I_{Na} traces similar to what could be obtained in experiments where TTX was used to isolate I_{Na}. Ideally, higher expression levels could be beneficial to 'minimize' I_{bck}, but are also unwanted because of voltage errors they would introduce. Whole-cell I_{Na} recordings at

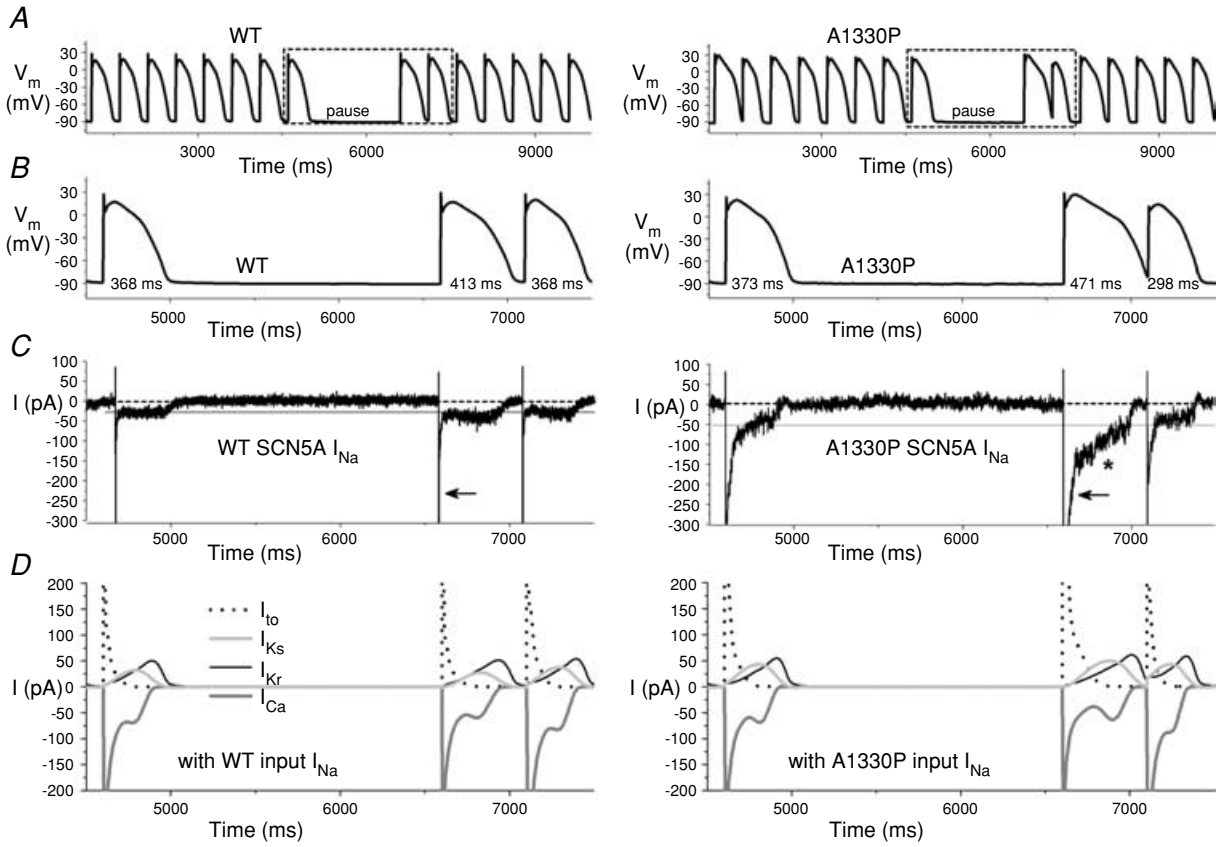

Figure 6. Prolonging effects of the A1330P mutation are reduced at fast stimulation rate
A, subepicardial cell APs generated with WT or A1330P I_{Na}, at 2 Hz. *B*, boxed APs from *A* and *C*, associated I_{Na}s. After a 2 s pause, late A1330P I_{Na} increases (*), resulting in a prolonged AP; note the slower time-course of peak A1330P I_{Na} inactivation compared to that of WT (arrows). *D*, selected associated individual membrane currents in the PB model cell.

physiological temperature are technically challenging due to fast (in)activation kinetics and large current amplitudes (Nagatomo *et al.* 1998; Dumaine *et al.* 1999; Wang *et al.* 2000; Rivolta *et al.* 2001; Keller *et al.* 2005). However, the importance of experimental temperatures approaching the physiological range is highlighted by findings that the electrophysiological profile at room temperature may not adequately explain the ECG signature (Dumaine *et al.* 1999). Similarly, the extent of a mutation-induced change on $Na_V1.5$ channel function can be masked at room temperature: enhancement of intermediate inactivation with the Y1795C mutant is undetected at room temperature, but augmented at 32°C (Rivolta *et al.* 2001). Our results reveal specific kinetic features of WT and mutant I_{Na} under close-to-physiological conditions, i.e. by recording at 35°C and letting I_{Na} generate and shape the ventricular AP. Regional AP heterogeneity due to intrinsic differences between cell types was reproduced by adjusting selected membrane ionic currents in the PB model cell and by implementing HEK cell I_{Na} to the PB model cell. The method allowed a close investigation of the effects of AP morphology on the time-course of I_{Na}. The studied mutations caused AP prolongations in all cell types studied. Our results on the Y1795C

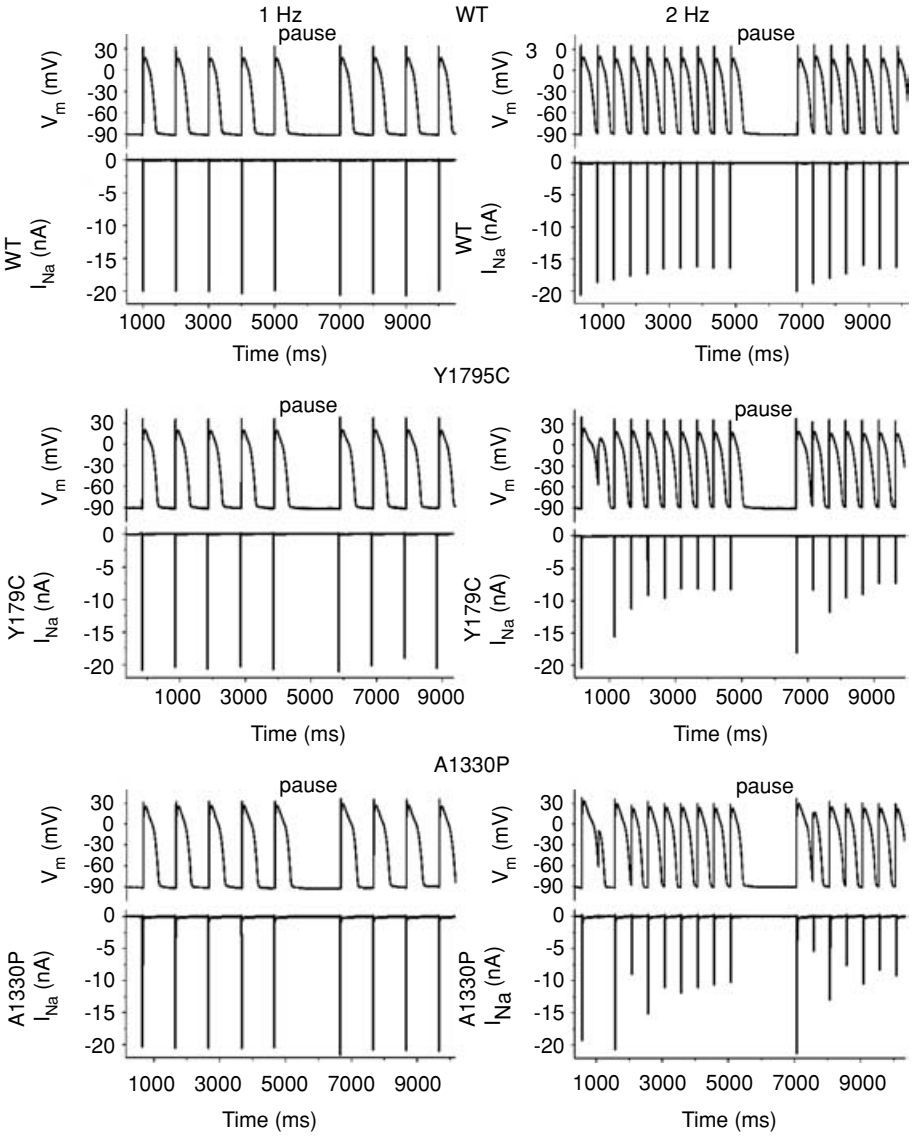

Figure 7. Representative examples of the effects of pacing rate and of a pause on WT or mutant peak I_{Na}s
APs were recorded from a 'subepicardial' cell successively coupled to HEK cells transfected with WT (top), Y1795C (middle) or A1330P (bottom) channels. A normal (WT) response is shown in the top panels, while APs in LQT syndrome are prolonged compared to normal (middle and bottom). At 2 Hz, after the pause, the extent of AP prolongation is exaggerated and heterogeneous. Note the corresponding I_{Na}s.

mutation confirm those of Clancy *et al.* (2002), though the resulting APD prolongation in dAPC experiments was more pronounced: a 35–88 ms increase for the Y1795C mutation at 0.5–2 Hz (Fig. 8) in contrast with the 10–30 ms predicted by computer simulations. Similarly, dAPC data on the A1330P mutant give an insight into the mechanism underlying AP prolongation and arrhythmogenesis in the carrier of this mutation. Facilitated (re)openings of the cardiac sodium channels due to mutation are likely to cause a rise in intracellular Na^+ concentration ($[Na^+]_i$), and, through increased plateau I_{Ca} (due to AP prolongation) as well as depressed Na^+/Ca^{2+} exchange, intracellular Ca^{2+} ($[Ca^{2+}]_i$). By calculating the charge, Q_{Na}, from the integral of the WT or mutant I_{Na} during the AP plateau and repolarization phases, the assumption that cells with mutant sodium channels have increased $[Na^+]_i$ values compared to WT can be corroborated (not shown). Besides, an increase of $[Ca^{2+}]_i$ by itself can give rise to delayed afterdepolarizations (DADs), which also are a substrate for arrhythmias.

Literature data suggest that sudden pauses play a major role in the genesis of spontaneous arrhythmias in the congenital LQT syndrome (Viskin *et al.* 2000). Patients with LQT3 are at a greater risk of cardiac events during rest or bradycardia than during exercise when heart rate is elevated (Clancy *et al.* 2002; Veldkamp *et al.* 2003). The onset of torsades de pointes arrhythmias in LQT3 tends to be bradycardia- or pause-dependent, contrary to other LQT syndromes that tend to be adrenergic dependent (Schwartz *et al.* 1995; Schwartz *et al.* 2001). Frequency-dependent changes of the late and peak I_{Na} were studied in detail only with the ΔKPQ mutant. There, rate-dependent reduction of late I_{Na} may account for the shortening of QT interval at higher rates (Nagatomo *et al.* 2002). In dAPC experiments, late I_{Na} amplitudes of Y1795C and A1330P mutants were strongly rate dependent, conducting less late I_{Na} at faster rates. Similarly, at fast rates, peak I_{Na} was more decreased with mutant channels, suggesting a 'more absorbing' intermediate inactivation in both cases, compared to the normal situation (WT). In addition to this, the increased AP durations in LQT3 further enhance intermediate inactivation during depolarizations and cause failure of channels to recover during the short hyperpolarizations between the pulses. At the same time, when APs are prolonged, currents through normal and unmodified channels are also modified (Figs 5*D*, 6*D* and 9). These currents further shape (by tending to prolong and/or shorten) the AP, supporting the concept of complex nature of interactions between different current components. Our dAPC data show that both mutations cause frequency- and pause-dependent changes of the AP and I_{Na} characteristics, and demonstrate that the I_{Na}, as well as other selected currents during the AP, not only depends on the instantaneous voltage alone, but depends upon the previous voltages before the applied AP-waveform as well. The pronounced effect of a pause after rapid pacing, combined with elevation of intracellular Ca^{2+} would provide an 'ideal breeding ground for afterdepolarizations, triggering, and heterogeneity of APDs that are thought to underlie torsades de pointes' (Roden & Anderson, 2000).

General considerations

The PB model of the cardiac AP (Priebe & Beuckelmann, 1998) does not include the late component exhibited by WT and mutant Na^+ channels. Description of currents in the PB model is based on results from voltage-clamp experiments, and the description of most membrane current components, but not the sodium current, is based on quantitative data from human ventricular cells.

PB model cell APs can exhibit early afterdepolarizations (EADs), but only with significantly enhanced I_{Ca}. This represents a shortcoming of all current human ventricular cell models (Priebe & Beuckelmann, 1998; Iyer *et al.* 2004; ten Tusscher *et al.* 2004). Experimental data demonstrate that voltage-dependent inactivation of the L-type Ca^{2+} current (I_{Ca}) occurs rather slowly, while Ca^{2+}-induced inactivation of I_{Ca} is much faster (Carmeliet, 2004). As discussed in detail by Iyer *et al.* (2004), human ventricular cell models require an artificial dominant voltage-dependent inactivation of I_{Ca} to assure AP stability. This dominant inactivation of I_{Ca} tends to prevent formation of EADs by inhibiting reactivation of I_{Ca} during the plateau phase of the AP.

Autonomic regulation is not implemented in the PB ventricular cell model. Such regulation would not only cause frequency-dependent changes but would also have additional effects on various ionic currents. For a

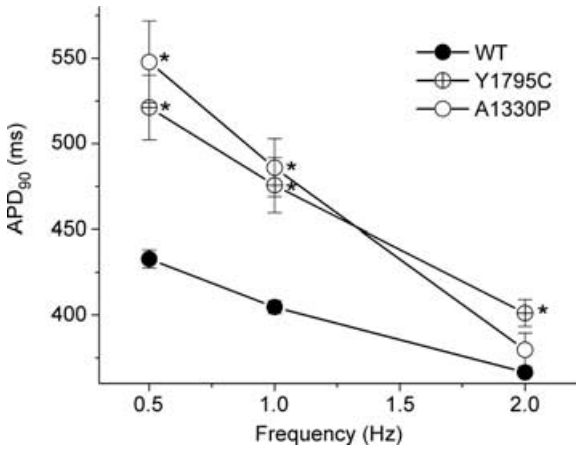

Figure 8. AP duration at 90% repolarization (APD_{90}) with the subepicardial cell with WT or mutant I_{Na}s
See Table 1 for *n* at 1 and 2 Hz; at 0.5 Hz *n* was ≥ 6 in all cases.
*Significant difference *versus* control ($P < 0.05$ for mutant *versus* WT).

number of years, transgenic mice proved to be suitable models in cardiovascular research, offering an adequate cellular environment to study autonomic influences on cardiac ion channels (Charpentier *et al.* 2004). For instance, the knock-in ΔKPQ mice show LQT3 features, including arrhytmogenicity (Nuyens *et al.* 2001). Although endogenous factors may influence the behaviour of the transgene, and extrapolation of results from mice to the human situation should be done circumspectly (London, 2001), these and similar models might help elucidate the pathophysiology of certain exercise- or emotion-triggered (Schwartz *et al.* 2001) LQT3 syndromes.

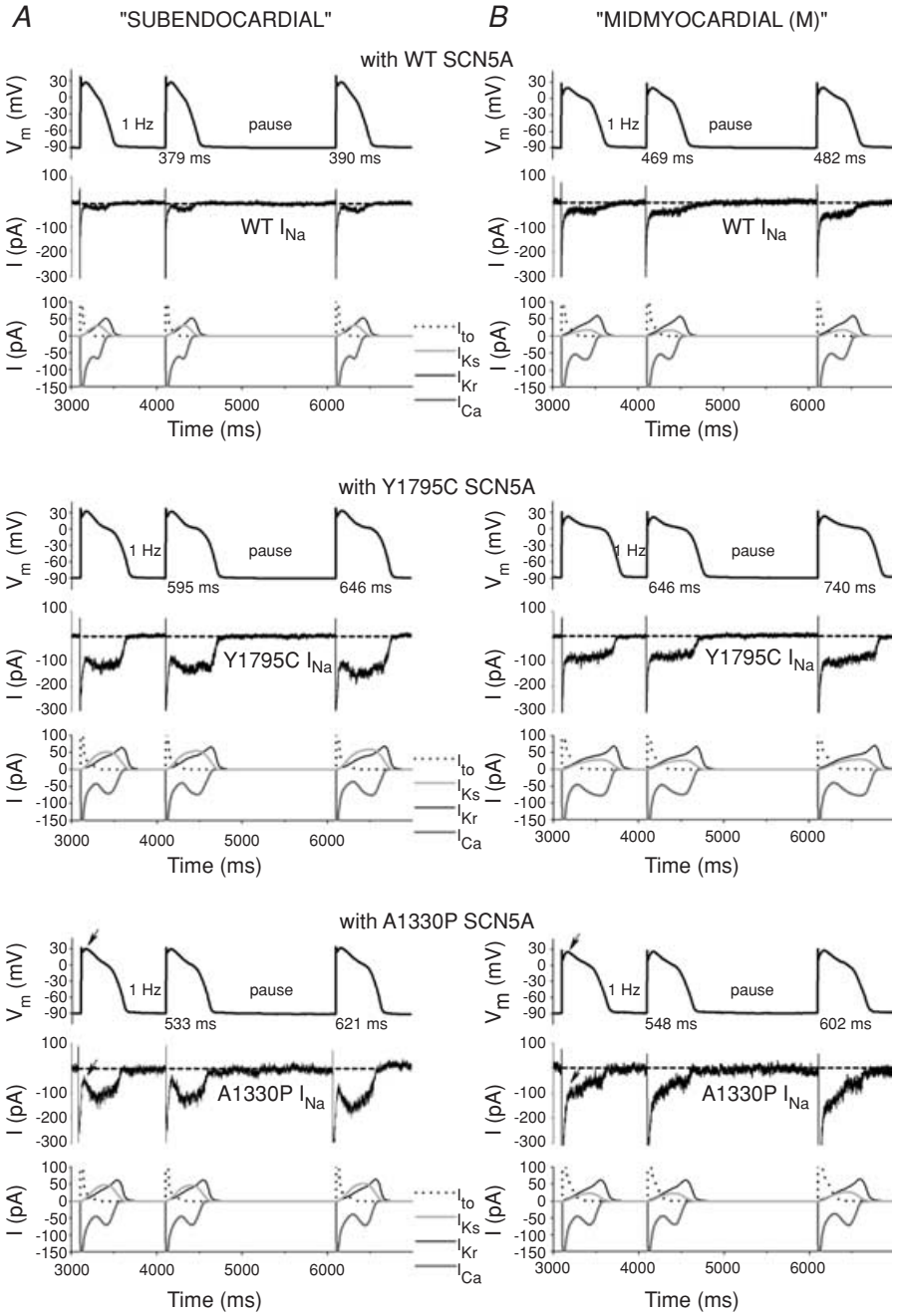

Figure 9. AP prolongation caused by the Y1795C and A1330P mutations in 'subendocardial' (*A*) and 'M' (*B*) cells

Representative APs (top) at 1 Hz, the corresponding HEK cell I_{Na} (middle), and associated individual membrane currents in the PB model cell (bottom). AP prolongation was exaggerated in subendocardial and M cells compared to subepicardial cells. The same input (WT, Y1795C, or A1330P) I_{Na} peak amplitude was used in *A* and *B*, respectively. Arrows in bottom panels indicate plateau amplitude and the corresponding late I_{Na} amplitude.

Although much effort was expended on tuning for optimum noise and speed, our attempts to establish dAPC in real-cell mode (HEK cell coupled to a freshly isolated rabbit left ventricular myocyte) were not successful because of instabilities and oscillatory distortions of the upscaled and I_{bck}-subtracted input I_{Na}. The shortcomings were probably related to imperfect C_m and/or R_s compensation when coupling two voltage-clamp amplifiers and/or to a delay during the dAPC time steps, occurring even when using an Alembic VE-2 amplifier (Alembic Instuments, Montreal, Quebec) with state estimator R_s compensation (Sherman *et al.* 1999). A major problem in connecting to a real ventricular cell is that fast-activating and large-amplitude (~40–60 nA, when upscaled) input I_{Na} might cause inhomogeneities of the membrane potential (V_m) of the real cell. Unfortunately, this cannot be improved with an expression system offering larger currents: as pointed out in the Electrophysiology section of the Methods, the larger the current, the more difficult it is to obtain reliable voltage control. A way out would be to combine 'conventional APC' to generate the upstroke and thereafter switch to dAPC with a slower, more stable feedback to study the I_{Na} during the plateau phase.

Conclusions

LQT3 syndrome is linked to mutations in the *SCN5A* gene. Despite this link, the mechanism by which a given mutation leads to the clinically observed electrical disease often remains obscure. We used close-to-physiological conditions to study AP morphology and the time-course and magnitude of late I_{Na} during the plateau and repolarizing phases of the AP. With mutant I_{Na}, APD was longer than with WT, due to a stimulation-frequency-dependent large late I_{Na} component. This late I_{Na} importantly contributes to the AP plateau and AP repolarization. Mid-myocardial cells exhibited pronounced AP prolongation compared to subepicardial cells, resulting in increased APD dispersion for each of the mutants. Thus, with the dAPC approach, we were able to demonstrate the effects of various clinically relevant stimulation frequencies as well the consequence of a pause on AP morphology, and to reveal the arrhythmogenic nature of LQT3-associated *SCN5A* mutations.

References

An RH, Wang XL, Kerem B, Benhorin J, Medina A, Goldmit M & Kass RS (1998). Novel LQT-3 mutation affects Na^+ channel activity through interactions between α- and β_1-subunits. *Circ Res* **83**, 141–146.

Bennett PB, Yazawa K, Makita N & George AL Jr (1995). Molecular mechanism for an inherited cardiac arrhythmia. *Nature* **376**, 683–685.

Berecki G, Zegers JG, Verkerk AO, Bhuiyan ZA, de Jonge B, Veldkamp MW, Wilders R & van Ginneken AC (2005). HERG channel (dys) function revealed by dynamic action potential clamp technique. *Biophys J* **88**, 566–578.

Carmeliet E (2004). Intracellular Ca^{2+} concentration and vate adaptatior of the cardiac action potential. *Cell Calcium* **35**, 557–573.

Catterall WA (2000). From ionic currents to molecular mechanisms: the structure and function of voltage-gated sodium channels. *Neuron* **26**, 13–25.

Charpentier F, Demolombe S & Escande D (2004). Cardiac channelopathies: from men to mice. *Ann Med* **36** (Suppl. 1), 28–34.

Clancy CE & Rudy Y (1999). Linking a genetic defect to its cellular phenotype in a cardiac arrhythmia. *Nature* **400**, 566–569.

Clancy CE, Tateyama M & Kass RS (2002). Insights into the molecular mechanisms of bradycardia-triggered arrhythmias in long QT-3 syndrome. *J Clin Invest* **110**, 1251–1262.

Clancy CE, Tateyama M, Liu H, Wehrens XH & Kass RS (2003). Non-equilibrium gating in cardiac Na^+ channels: an original mechanism of arrhythmia. *Circulation* **107**, 2233–2237.

Dumaine R, Towbin JA, Brugada P, Vatta M, Nesterenko DV, Nesterenko VV, Brugada J, Brugada R & Antzelevitch C (1999). Ionic mechanisms responsible for the electrocardiographic phenotype of the Brugada syndrome are temperature dependent. *Circ Res* **85**, 803–809.

Franz MR, Schaefer J, Schottler M, Seed WA & Noble MI (1983). Electrical and mechanical restitution of the human heart at different rates of stimulation. *Circ Res* **53**, 815–822.

Helix N, Strobaek D, Dahl BH & Christophersen P (2003). Inhibition of the endogenous volume-regulated anion channel (VRAC) in HEK293 cells by acidic di-aryl-ureas. *J Membr Biol* **196**, 83–94.

Iyer V, Mazhari R & Winslow RL (2004). A computational model of the human left-ventricular epicardial myocyte. *Biophys J* **87**, 1507–1525.

Jiang C, Atkinson D, Towbin JA, Splawski I, Lehmann MH, Li H, Timothy K, Taggart RT, Schwartz PJ, Vincent GM, Moss AJ & Keating MT (1994). Two long QT syndrome loci map to chromosomes 3 and 7 with evidence for further heterogeneity. *Nat Genet* **8**, 141–147.

Keller DI, Rougier JS, Kucera JP, Benammar N, Fressart V, Guicheney P, Madle A, Fromer M, Schlapfer J & Abriel H (2005). Brugada syndrome and fever: Genetic and molecular characterization of patients carrying SCN5A mutations. *Cardiovasc Res* **67**, 510–519.

London B (2001). Cardiac arrhythmias: from (transgenic) mice to men. *J Cardiovasc Electrophysiol* **12**, 1089–1091.

Magyar J, Kiper CE, Dumaine R, Burgess DE, Bányász T & Satin J (2004). Divergent action potential morphologies reveal nonequilibrium properties of human cardiac Na^+ channels. *Cardiovasc Res* **64**, 477–487.

Maltsev VA, Sabbah HN, Higgins RS, Silverman N, Lesch M & Undrovinas AI (1998). Novel, ultraslow inactivating sodium current in human ventricular cardiomyocytes. *Circulation* **98**, 2545–2552.

Moss AJ, Zareba W, Benhorin J, Locati EH, Hall WJ, Robinson JL, Schwartz PJ, Towbin JA, Vincent GM & Lehmann MH (1995). ECG T-wave patterns in genetically distinct forms of the hereditary long QT syndrome. *Circulation* **92**, 2929–2934.

Nagatomo T, Fan ZYeB, Tonkovich GS, January CT, Kyle JW & Makielski JC (1998). Temperature dependence of early and late currents in human cardiac wild-type and long Q-T ΔKPQ Na^+ channels. *Am J Physiol* **275**, H2016–H2024.

Nagatomo T, January CTYeB, Abe H, Nakashima Y & Makielski JC (2002). Rate-dependent QT shortening mechanism for the LQT3 ΔKPQ mutant. *Cardiovasc Res* **54**, 624–629.

Nuyens D, Stengl M, Dugarmaa S, Rossenbacker T, Compernolle V, Rudy Y, Smits JF, Flameng W, Clancy CE, Moons L, Vos MA, Dewerchin M, Benndorf K, Collen D, Carmeliet E & Carmeliet P (2001). Abrupt rate accelerations or premature beats cause life-threatening arrhythmias in mice with long-QT3 syndrome. *Nat Med* **7**, 1021–1027.

Priebe L & Beuckelmann DJ (1998). Simulation study of cellular electric properties in heart failure. *Circ Res* **82**, 1206–1223.

Rivolta I, Abriel H, Tateyama M, Liu H, Memmi M, Vardas P, Napolitano C, Priori SG & Kass RS (2001). Inherited Brugada and long QT-3 syndrome mutations of a single residue of the cardiac sodium channel confer distinct channel and clinical phenotypes. *J Biol Chem* **276**, 30623–30630.

Rivolta I, Clancy CE, Tateyama M, Liu H, Priori SG & Kass RS (2002). A novel SCN5A mutation associated with long QT-3: altered inactivation kinetics and channel dysfunction. *Physiol Genomics* **10**, 191–197.

Roden DM & Anderson ME (2000). The pause that refreshes, or does it? Mechanisms in torsades de pointes. *Heart* **84**, 235–237.

Ruff RL (1998). Cells use the singular properties of different channels to produce unique electrical songs. *Biophys J* **74**, 2745–2746.

Schwartz PJ, Priori SG, Locati EH, Napolitano C, Cantu F, Towbin JA, Keating MT, Hammoude H, Brown AM & Chen LS (1995). Long QT syndrome patients with mutations of the *SCN5A* and *HERG* genes have differential responses to Na^+ channel blockade and to increases in heart rate. Implications for gene-specific therapy. *Circulation* **92**, 3381–3386.

Schwartz PJ, Priori SG, Spazzolini C, Moss AJ, Vincent GM, Napolitano C, Denjoy I, Guicheney P, Breithardt G, Keating MT, Towbin JA, Beggs AH, Brink P, Wilde AA, Toivonen L, Zareba W, Robinson JL, Timothy KW, Corfield V, Wattanasirichaigoon D, Corbett C, Haverkamp W, Schulze-Bahr E, Lehmann MH, Schwartz K, Coumel P & Bloise R (2001). Genotype-phenotype correlation in the long–QT syndrome: gene-specific triggers for life-threatening arrhythmias. *Circulation* **103**, 89–95.

Sherman AJ, Shrier A & Cooper E (1999). Series resistance compensation for whole-cell patch-clamp studies using a membrane state estimator. *Biophys J* **77**, 2590–2601.

Sigworth FJ (1983). Electronic design of the patch clamp. In *Single-Channel Recording*, ed. Sakmann B, Neher E, pp. 3–35. Plenum Press, New York.

Smits JP, Veldkamp MW, Bezzina CR, Bhuiyan ZA, Wedekind H, Schulze-Bahr E & Wilde A (2005). Substitution of a conserved alanine in the domain IIIS4–S5 linker of the cardiac sodium channel causes long QT syndrome. *Cardiovasc Res* **67**, 459–466.

ten Tusscher KH, Noble D, Noble PJ & Panfilov AV (2004). A model for human ventricular tissue. *Am J Physiol Heart Circ Physiol* **286**, H1573–H1589.

Veldkamp MW, Wilders R, Baartscheer A, Zegers JG, Bezzina CR & Wilde AA (2003). Contribution of sodium channel mutations to bradycardia and sinus node dysfunction in LQT3 families. *Circ Res* **92**, 976–983.

Viskin S, Fish R, Zeltser D, Belhassen B, Heller K, Brosh D, Laniado S & Barron HV (2000). Arrhythmias in the congenital long QT syndrome: how often is torsade de pointes pause dependent? *Heart* **83**, 661–666.

Wang DW, Makita N, Kitabatake A, Balser JR & George AL Jr (2000). Enhanced Na^+ channel intermediate inactivation in Brugada syndrome. *Circ Res* **87**, E37–E43.

Wang Q, Shen J, Splawski I, Atkinson D, Li Z, Robinson JL, Moss AJ, Towbin JA & Keating MT (1995). SCN5A mutations associated with an inherited cardiac arrhythmia, long QT syndrome. *Cell* **80**, 805–811.

Wedekind H, Smits JP, Schulze-Bahr E, Arnold R, Veldkamp MW, Bajanowski T, Borggrefe M, Brinkmann B, Warnecke I, Funke H, Bhuiyan ZA, Wilde AA, Breithardt G & Haverkamp W (2001). *De novo* mutation in the *SCN5A* gene associated with early onset of sudden infant death. *Circulation* **104**, 1158–1164.

Wehrens XH, Vos MA, Doevendans PA & Wellens HJ (2002). Novel insights in the congenital long QT syndrome. *Ann Intern Med* **137**, 981–992.

Wilders R (2005). 'Dynamic clamp' in cardiac electrophysiology. *J Physiol* **566**, 641.

Zaniboni M, Pollard AE, Yang L & Spitzer KW (2000). Beat-to-beat repolarization variability in ventricular myocytes and its suppression by electrical coupling. *Am J Physiol Heart Circ Physiol* **278**, H677–H687.

Acknowledgements

We thank Berend de Jonge for excellent assistance with the HEK-293 cell culture. This study was supported by Netherlands Heart Foundation Grant 2001B155.

Supplemental material

The online version of this paper can be accessed at:
DOI: 10.1113/jphysiol.2005.096578
http://jp.physoc.org/cgi/data/jphysiol.2005.096578/DC1
and contains supplemental material including four figures entitled:

Figure S1: The effects of reducing model cell I_{Na} density on the AP duration.

Figure S2: Late I_{Na} magnitude during depolarising ramps depends on the duration of the depolarising voltage prepulse.

Figure S3: I_{bck} substration in the presence of Y1795C input I_{Na}.

Figure S4: Ap heterogeneity and mutation-induced dispersion of AP duration in dAPC experiments.

This material can also be found as part of the full-text HTML version available from http://www.blackwell-synergy.com